



Metabolic interplay drives population cycles in a cross-feeding microbial community

Received: 4 October 2024

Accepted: 4 September 2025

Published online: 07 October 2025

Tyler D. Ross^{1,2}, Hanhyeok Im³, Brennan G. Keogh³,
Christopher A. Klausmeier^{4,5,6,7}  & Ophelia S. Venturelli^{1,2,3,8,9} 

Population cycles are prevalent in ecosystems and play key roles in determining their functions. While multiple mechanisms have been theoretically shown to generate population cycles, there are limited examples of mutualisms driving self-sustained oscillations. Using an engineered microbial community that cross-feeds essential amino acids, we experimentally demonstrate cycles in strain abundance that are robust across environmental conditions. A nonlinear dynamical model that incorporates the experimentally observed cross-inhibition of amino acid production recapitulates the population cycles. The model shows that the cycles represent internally generated relaxation oscillations, which emerge when fast resource dynamics with positive feedback drive slow changes in strain abundance. The temporal structure of the resource dynamics prevents nonproducing cheaters from persisting within the oscillating community. Our findings highlight the critical role of resource dynamics and feedback in shaping population cycles in microbial communities and have implications for biotechnology.

Population cycles (regular oscillations in population size) are widespread in ecological systems, with almost 30% of natural populations showing such dynamics¹. Many mechanisms have been proposed to explain how internally generated oscillations can emerge from nonlinear interactions between populations. Beginning with Lotka and Volterra's foundational predator-prey model^{2,3}, consumer-resource (+/-) interactions have been shown to be a common cause of population cycles⁴. Other theoretical mechanisms that can generate regular oscillations include age- and stage-structure⁵, intransitive competition⁶, and eco-evolutionary dynamics⁷.

Mutualism (+/+) is increasingly recognized as a pervasive and influential interaction motif shaping diverse ecosystems^{8–10}. Mutualistic interactions can give rise to nonlinear phenomena such as alternative stable states¹¹. However, this interaction motif has not been widely considered a driver of oscillatory dynamics, though a few cases

have been recently found^{12,13}. Mutualisms were first modeled using the generalized Lotka-Volterra model¹⁴, but this model can generate unbounded growth and instability¹⁵. In more recent models, the mechanisms driving mutualisms are a central focus, particularly among interacting macroscopic organisms¹⁶. Mutualisms are also present in microbial communities, whose interactions influence a broad range of natural phenomena from biogeochemical cycles to human health and behavior^{17,18}. Cross-feeding, a mechanism of mutual resource exchange, is frequently observed in microbial communities^{19–23}. Previous experimental studies have shown that cross-feeding can stabilize co-cultures, but these studies typically rely on endpoint measurements and do not capture dynamic behaviors such as population cycles²⁴. Consistent with the theoretical understanding that mutualisms lead to stable equilibria, current models of cross-feeding mutualisms do not exhibit population cycles²⁵.

¹Department of Biomedical Engineering, University of Wisconsin-Madison, Madison, WI, USA. ²Department of Biochemistry, University of Wisconsin-Madison, Madison, WI, USA. ³Department of Biomedical Engineering, Duke University, Durham, NC, USA. ⁴W. K. Kellogg Biological Station, Michigan State University, Hickory Corners, MI, USA. ⁵Program in Ecology, Evolution and Behavior, Michigan State University, East Lansing, MI, USA. ⁶Department of Plant Biology, Michigan State University, East Lansing, MI, USA. ⁷Department of Integrative Biology, Michigan State University, East Lansing, MI, USA. ⁸Department of Chemical and Biological Engineering, University of Wisconsin-Madison, Madison, WI, USA. ⁹Department of Bacteriology, University of Wisconsin-Madison, Madison, WI, USA. ✉ e-mail: klausme@msu.edu; ophelia.venturelli@duke.edu

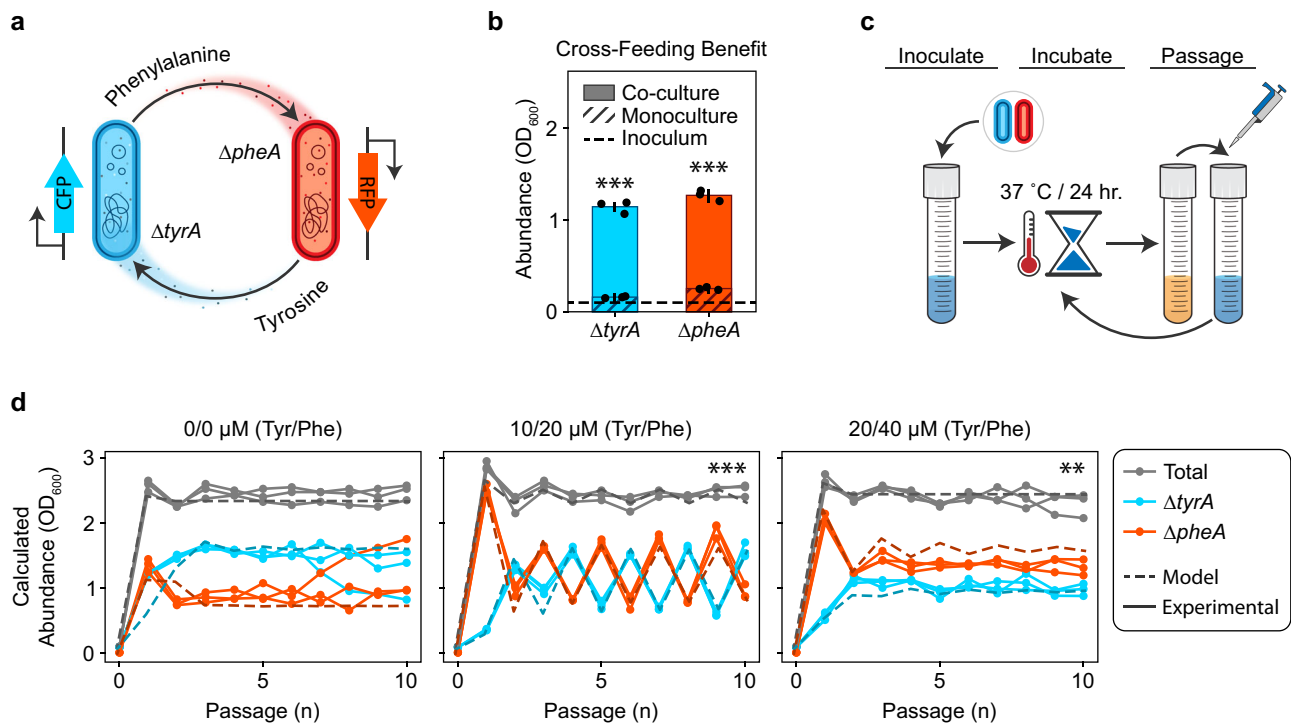


Fig. 1 | An amino acid cross-feeding microbial community displays stable equilibrium or oscillatory dynamics. **a** Two *E. coli* amino acid auxotrophs exhibit mutually beneficial cross-feeding. Mutant *ΔtyrA* produces phenylalanine that enables the growth of mutant *ΔpheA*, while mutant *ΔpheA* reciprocally produces tyrosine to enable the growth of mutant *ΔtyrA*. Each auxotroph harbors an IPTG-inducible fluorescent reporter for strain identification and abundance quantitation in co-culture. **b** Relative growth benefit due to cross-feeding. Auxotrophs *ΔtyrA* and *ΔpheA* were grown as monocultures and as a pairwise community in minimal medium lacking any amino acid supplementation ($n=3$, biological replicates). The absolute abundance after 24 h of growth for each monoculture is shown with hash-filled bars. The calculated absolute abundance (OD₆₀₀ multiplied by the relative abundance) after 24 h of growth for each member in the pairwise community is shown with solid bars. Error bars indicate one standard deviation from the mean for each culture. The inoculum density is shown as a dashed line. Individual datapoints are shown as black dots. Asterisks indicate statistical significance between the average growth in monoculture versus co-culture (*ΔtyrA*: $p=1.5220e-05$, $g^*=-16.3237$; *ΔpheA*: $p=7.8113e-06$, $g^*=-19.3008$). **c** In the experimental passinging scheme, we inoculated a pair of cross-feeding amino acid auxotrophs into a minimal or supplemented media. The culture is incubated for a period of 24 h prior to being diluted to a constant OD₆₀₀. Cycles of growth and dilution are carried forward for a finite number of passages. **d** Dynamical behaviors of the *ΔtyrA*, *ΔpheA* community when subjected to the experimental passinging scheme ($n=3$, biological replicates). Separate plots correspond with different concentrations of amino acid supplementation in the passinging media. Gray lines indicate the total biomass of the community while colored lines indicate the calculated absolute abundance (OD₆₀₀ multiplied by the relative abundance) of *ΔtyrA* (cyan) or *ΔpheA* (red). Solid lines with circular markers represent experimental data and dashed lines represent simulations of equation (1) for which $\tau=24$ h (as in batch culture). Asterisks indicate statistical significance in a test for period-two oscillations (0/0: $p=0.8522$, $g^*=0.0443$; 10/20: $p=7.4249e-11$, $g^*=-8.3648$; 20/40: $p=0.0035$, $g^*=-1.5345$) (Methods). Raw data for panels (b) and (d) are provided in the Source Data file.

Here, we demonstrate that an engineered microbial community shaped by bidirectional cross-feeding of essential amino acids can exhibit robust population cycles across a range of environmental conditions. Our study builds on and extends previous work^{22,24} by capturing the dynamic nature of mutualistic cross-feeding interactions. Resource profiling demonstrates a pattern of amino acid cross-inhibition that has not been previously captured in models of mutualisms. A nonlinear dynamical systems model that encodes the observed mutual resource inhibition replicates the observed dynamics and can accurately extrapolate to new environmental conditions. Our models demonstrate that the cycles emerge as internally generated relaxation oscillations, where the fast mutual inhibition of amino acid production (positive feedback) leads to alternative stable states, which drive slow population dynamics. We further demonstrate that the population cycling can exclude a nonproducing cheater via temporal patterning of the resource environment. Our results demonstrate that resource-mediated interactions in microbial communities can generate rich dynamical behaviors and have implications for innovations in biotechnology.

Results

Microbial communities driven by amino acid cross-feeding can exhibit distinct dynamical behaviors

To investigate how cross-feeding shapes community dynamics, we engineered individual *Escherichia coli* (*E. coli*) amino acid auxotrophs *ΔtyrA* and *ΔpheA* that reciprocally cross-feed phenylalanine and tyrosine respectively, while competing for glucose (Fig. 1a). Relative to other amino acid auxotroph pairs, the *ΔtyrA* and *ΔpheA* co-culture showed a particularly strong benefit due to cross-feeding²⁴, where monocultures exhibited minimal growth and co-cultures displayed significant growth after 24 h in media lacking amino acids (Fig. 1b). This shows that cross-feeding plays a critical role in structuring communities in environments lacking external supply of the required amino acids.

To investigate the dynamics of the community, we co-cultured the strains in serial batches subjected to daily dilution with fresh media for 10 days. We supplemented the media at each passage with no, low, and moderate levels of external amino acid to modulate the obligation for cross-feeding (Fig. 1c). With no or moderate external amino acid supply, the composition of the communities converged to an equilibrium

(Fig. 1d). Notably, the community exhibited sustained large-amplitude period-two oscillations in the presence of low concentrations of external amino acids. The oscillations persisted in co-cultures regardless of the fluorescent protein expressed by each strain (Supplementary Fig. 1). To evaluate the robustness of these dynamics to variation in environmental parameters, the supplied concentration of amino acids was varied across a wide range. The community displayed period-two oscillations across a range of intermediate amino acid supply concentrations (Supplementary Fig. 2). These results demonstrate that oscillatory dynamics can emerge in microbial communities whose dominant interaction is resource cross-feeding, which is exceedingly rare in systems driven by a mutualism. In the presence of high and low initial phenylalanine supply and tyrosine supply, respectively, $\Delta tyrA$ was excluded. This implies that the contribution of mutualism versus resource competition was context dependent²⁶.

Tyrosine and phenylalanine release primarily occurs during focal amino acid starvation

Given that mainstream ecological models of mutualism do not account for oscillations, the presence of population cycles in the cross-feeding community implies that additional feedback mechanisms are required to produce them. Extant models of cross feeding that do not produce oscillations assume that nutrients are released at constant rates^{25,27}. In accordance with previous results that demonstrate a time-dependent change in the release of certain metabolites^{28,29}, we hypothesized that there exists unresolved feedback shaping the dynamics of amino acid release rates. Therefore, we measured the concentrations of extracellular resources (amino acids and glucose) over time for each auxotroph in response to varying supplementation of the required amino acid (Fig. 2a).

In the presence of high amino acid supplementation, a residual amount remained at the onset of stationary phase as glucose was depleted (Fig. 2b, e). In these cases of glucose limitation, almost none of the partner's amino acid was released at 12 h, and only a small amount was released at 24 h, likely due to cell death and lysis³⁰. Conversely, the required amino acid was completely depleted in stationary phase when lower amino acid concentrations were initially supplied. A moderate amount of remaining glucose indicated that these cultures were amino acid limited as opposed to glucose limited (with some exception at 24 h, see Supplementary Note 1). Notably, for both $\Delta tyrA$ and $\Delta pheA$, the limitation of required amino acid was associated with a substantial release of the partner strain's required amino acid (Fig. 2c, d, f, g). These results demonstrate significant reciprocal inhibition of amino acid release, where tyrosine inhibits release of phenylalanine by $\Delta tyrA$ and the reciprocal (Fig. 2h, i). Therefore, the cross-inhibitory interactions generate a positive feedback loop in the resource dynamics. When a given auxotroph is limited by its required amino acid, it releases the partner's required amino acid (producer). This leads to glucose limitation of the partner strain as opposed to amino acid limitation, preventing the reciprocal release of amino acid (consumer). Amino acid limitation of the producer is thus reinforced through a net positive feedback loop due to the cross-inhibition topology.

A dynamic model capturing resource and strain dynamics recapitulates system behaviors

To determine if the cross-inhibition of amino acid release can explain the emergence of oscillatory dynamics in our engineered community, we constructed a nonlinear ordinary differential equation model of the system. Our model considers two auxotrophs ($\Delta tyrA$ and $\Delta pheA$, denoted N_1 and N_2 , Eqs. (1a) and (1b)), two cross-fed resources (phenylalanine and tyrosine, denoted R_1 and R_2 , Eq. (1c) and (1d)) and one resource that ultimately limits the growth of the community (glucose, denoted R_3 , Eq. (1e))²⁵. Each auxotroph i has two essential resources (its required amino acid and glucose), with its realized growth rate μ_i given by the minimum of its potential growth on the two resources j ,

$\mu_{ij}(R_j)$, which take Michaelis-Menten form (Eqs. (1f) and (1g)) with half saturation constants k_{ij} . The maximum growth rate is denoted as $\mu_{i, \max}$. Amino acid uptake is proportional to the realized growth rate of the auxotrophs, while glucose uptake is proportional to their glucose-limited growth rate. The stoichiometric coefficients q_{ij} describe the amount of resource needed per unit of cell growth. We assume auxotrophs produce amino acid to match their glucose uptake and release any excess to the environment at rate $q_{ii}(\mu_{i3} - \mu_i)$. By contrast, when growth is glucose-limited, $\mu_i = \mu_{i3}$, and amino acids are not released into the environment. This mass-balance constraint leads to amino acid release only when glucose is available and the required amino acid limits growth, consistent with our experimental results (Fig. 2b–g).

We model the external supply of resources with concentration $R_{j, \text{in}}$ and dilution of species and resources at rate D . For comparison with our experimental results, we initially treat the dilution rate as a series of discrete events using $D(t) = f \sum_{n=1} \delta(t - n\tau)$, where f is the fraction of culture transferred, n is the passage number, τ is the period, and $\delta(\cdot)$ is the Dirac delta function. For further theoretical exploration, we treat the dilution rate D as a constant, as in a chemostat. Together, these assumptions yield the following model:

$$\frac{dN_1}{dt} = \mu_1 N_1 - DN_1 \quad (1a)$$

$$\frac{dN_2}{dt} = \mu_2 N_2 - DN_2 \quad (1b)$$

$$\frac{dR_1}{dt} = D(R_{1, \text{in}} - R_1) + q_{11}(\mu_{13} - \mu_1)N_1 - \mu_2 q_{21}N_2 \quad (1c)$$

$$\frac{dR_2}{dt} = D(R_{2, \text{in}} - R_2) + q_{22}(\mu_{23} - \mu_2)N_2 - \mu_1 q_{12}N_1 \quad (1d)$$

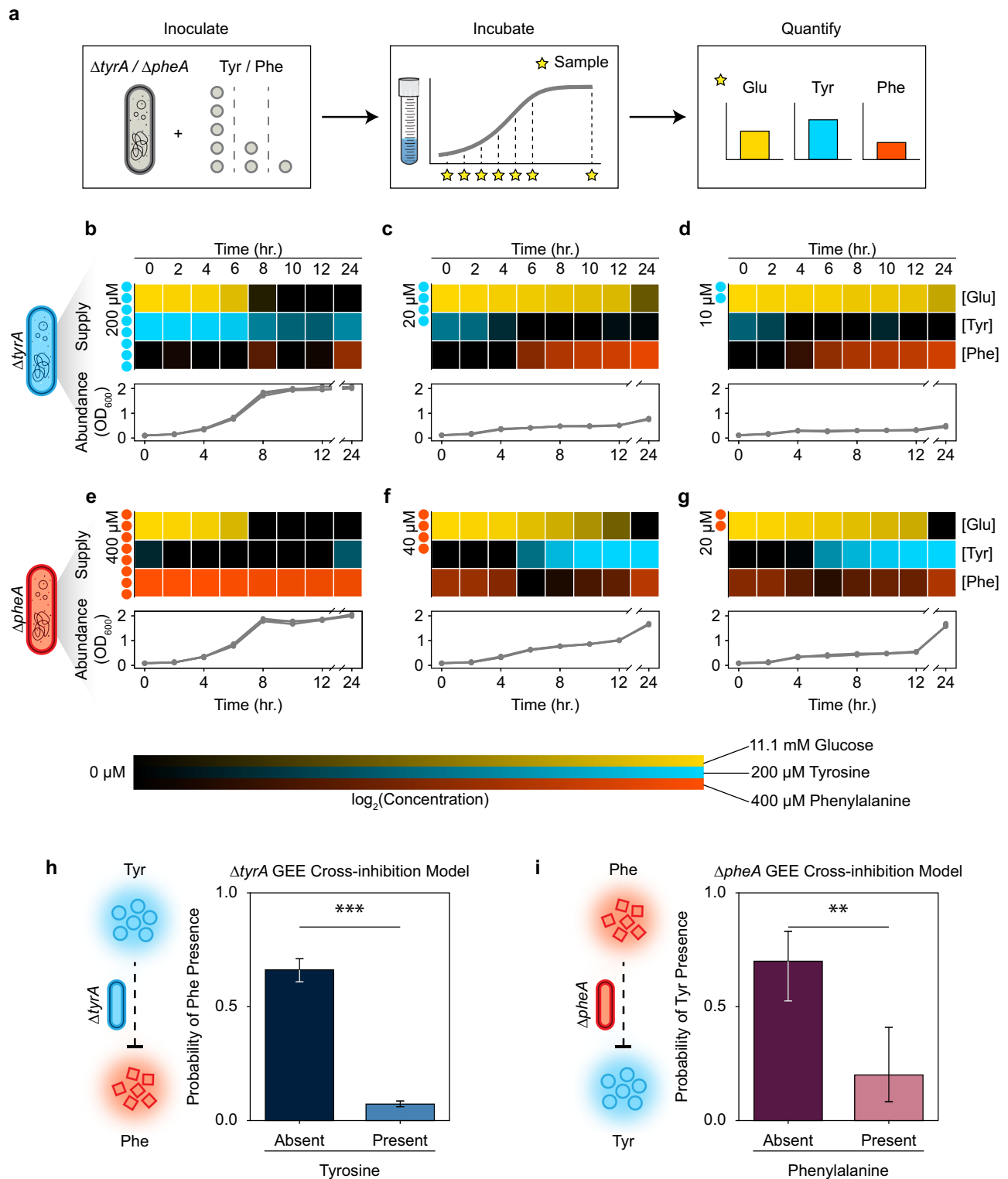
$$\frac{dR_3}{dt} = D(R_{3, \text{in}} - R_3) - \mu_{13} q_{13}N_1 - \mu_{23} q_{23}N_2 \quad (1e)$$

$$\mu_1 = \min(\mu_{12}(R_2), \mu_{13}(R_3)), \mu_2 = \min(\mu_{21}(R_1), \mu_{23}(R_3)) \quad (1f)$$

$$\mu_{ij}(R_j) = \mu_{i, \max} \frac{R_j}{R_j + k_{ij}} \quad (1g)$$

Further details about the model parameters are provided in Supplementary Table 1.

We inferred the model parameters using measurements of absolute abundance from our initial ten-batch passaging experiment (Methods) and cross-validation with short term passaging data over a range of amino acid supply concentrations (Supplementary Fig. 2). Our model (in discrete batch form) and best parameter estimate accurately fit the different dynamical behaviors as a function of amino acid supply concentration (Fig. 1d). Notably, the model accurately predicted the dynamical behaviors for the single-batch growth dynamics of a cycling community that were not used for fitting of the model (Supplementary Fig. 3). Therefore, the model can extrapolate to new environments. These results suggest that cross-feeding with reciprocal inhibition can generate the period-two cycles observed experimentally. We also explored an alternative model that uses predicted regulatory links at the biomolecular level (Supplementary Fig. 4) to encode a more explicit mechanism of resource cross inhibition^{31–34}. This alternative model could recapitulate the period-two cycles and equilibrium dynamics as a function of the amino acid supply concentrations (Supplementary Note 2 and Supplementary Fig. 5). This implies that the resource cross-inhibition topology was critical for generating oscillations in the system.



Cycles can result from external forcing or be self-sustained due to internal mechanisms driving the dynamics³⁵. For example, periodic forcing through daily passaging was necessary for the development of cycles in a mutualistic cross-protection microbial community¹³. To determine whether cycles can emerge in the absence of external forcing, we analyzed our model with constant dilution rate D as in a chemostat (Fig. 3a). Our results show that periodic limit-cycle solutions occur across a range of low external amino acid supply (Fig. 3b). This suggests that the experimentally observed cycles are not

dependent on periodic forcing through daily passaging but arise due to the internal dynamics of the community. Consistent with this result, the community displayed period-three cycles in a pseudo-continuous culture experiment in which the batch duration was decreased to 4 h (Supplementary Fig. 6). This further suggests a complex interplay between periodic external forcing and the internal dynamics. The connection between the periodically forced batch culture model (Fig. 1d) and the continuous chemostat model (Fig. 3) is explored in Supplementary Note 3.

Fig. 2 | Extracellular metabolite measurements demonstrate that amino acid release occurs in response to amino acid limitation. **a** Experimental design to analyze the extracellular dynamics of essential auxotroph resources. Each auxotroph was grown as a monoculture ($n = 3$, biological replicates) in media with either 200 μM , 20 μM , or 10 μM tyrosine for ΔtyrA , or 400 μM , 40 μM , or 20 μM phenylalanine for ΔpheA . Cultures were sampled every 2 h over a 12-h period, and again at 24 h. Glucose, tyrosine, and phenylalanine concentrations were quantified using fluorometric and colorimetric assays. **b–g** Extracellular resource dynamics in auxotroph monocultures. Line plots represent growth curves at different concentrations of amino acid supplementation, while heatmaps depict corresponding extracellular resource concentrations. Panels (**b–d**) show ΔtyrA monocultures, and (**e–g**) show ΔpheA monocultures. The initial amino acid supplementation levels (tyrosine for ΔtyrA and phenylalanine for ΔpheA) are indicated to the left of each heatmap. Heatmap shading indicates the concentrations of glucose (yellow),

tyrosine (cyan), and phenylalanine (red). Raw data for **b–g** are included in the Source data file. **h, i** Predicted probability of partner amino acid presence as a function of required amino acid availability. Predictions were made using a generalized estimating equation (GEE) with a binomial response model. The models were fit independently for ΔtyrA monoculture (**h**, $n = 3$, biological replicates) and ΔpheA monoculture (**i**, $n = 3$, biological replicates) data. Each bar represents the predicted probability of detecting released amino acid when the required amino acid is absent (left) or present (right), based on binary categorization of amino acid concentrations using the experimental limit of detection (LOD). Error bars indicate 95% confidence intervals derived from each model's estimated standard errors. Asterisks indicate a statistically significant change in the predicted presence of released amino acid as the availability of required amino acid switches from absent to present (ΔtyrA (**h**): $p = 1.7060\text{e} - 111$; ΔpheA (**i**): $p = 0.0013$).

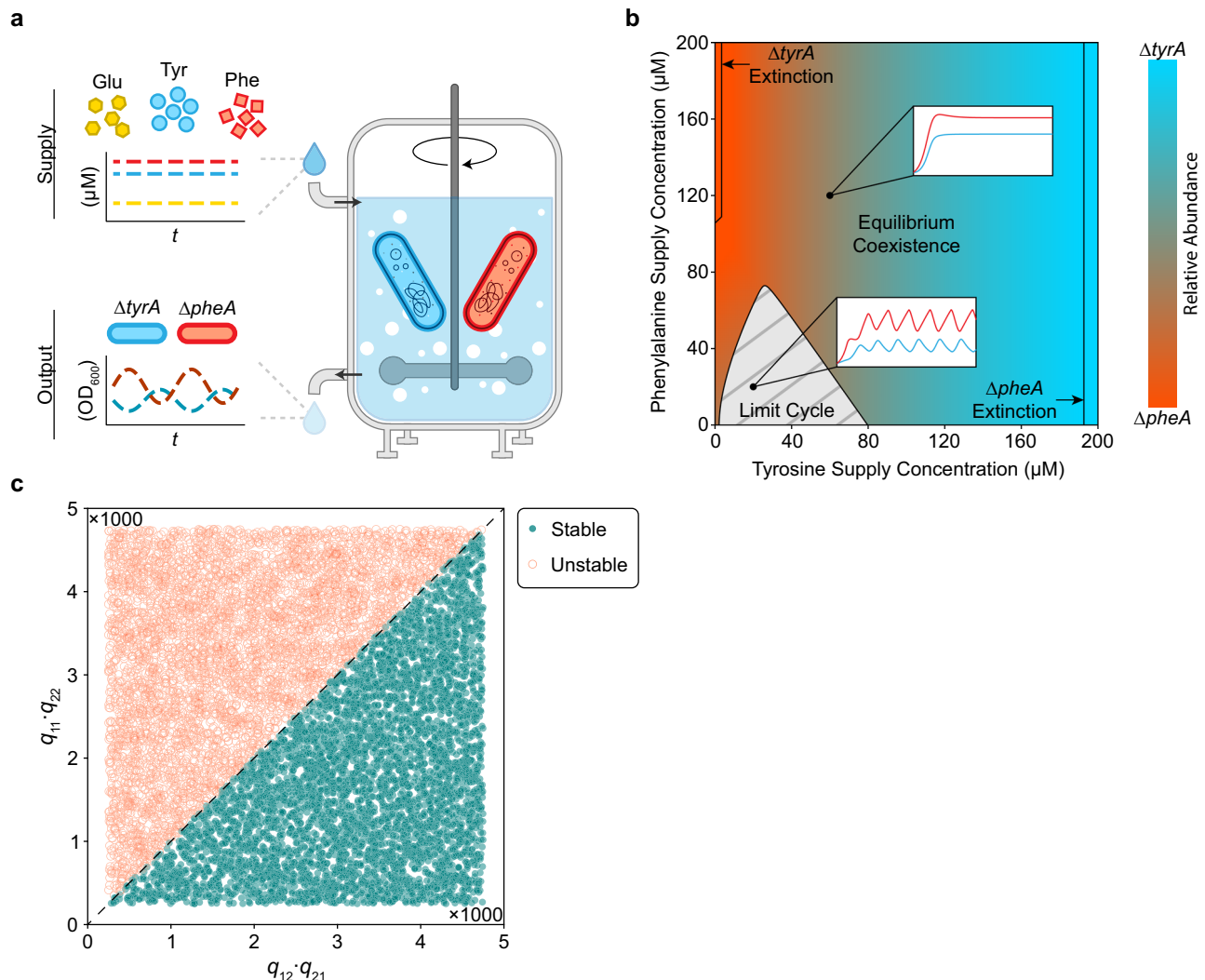


Fig. 3 | Population cycles exist in the absence of external forcing. **a** Schematic representation of the in silico chemostat experiment. The chemostat facilitates continuous growth of the ΔtyrA , ΔpheA community through constant inflow of glucose, tyrosine, and phenylalanine. Perfusion is governed by the dilution rate D , which acts on the inflow of external resource, and the outflow of chemostat resource and excess cells. **b** Two-dimensional bifurcation diagram of the ΔtyrA , ΔpheA community dynamics in a virtual chemostat. As the amino acid supply concentrations vary along each axis, the steady state community composition is indicated according to the color bar. A gray hashed region indicates the amino acid supply concentrations that do not produce stable equilibria but instead display limit cycle oscillations.

Transcritical bifurcations beyond which the community collapses into a monoculture are indicated with solid black lines. Two inset plots demonstrate simulations of stable equilibrium and cycling dynamics. **c** Steady state stability for randomly sampled values of q_{ij} . Stability analysis by analyzing the Jacobian matrix was used to determine the steady state stability for a range of $q_{11}q_{22}$ and $q_{12}q_{21}$ from 250 to 4750. Each point in the scatter plot represents the stability of a steady state for a given parameter sample. Filled in blue points represent stable steady states, while empty orange circles represent unstable steady states. A black line separates the region where $q_{11}q_{22} > q_{12}q_{21}$.

In our model, higher amino acid supply concentrations lead to stable equilibria, with a substantial range of parameters leading to stable coexistence of the auxotrophs (Fig. 3b). However, competitive exclusion occurs at extreme supply concentrations, and the outcome of this competition is solely sensitive to tyrosine supply as opposed to the tyrosine-to-phenylalanine supply ratio³⁶. This reflects the $\Delta tyrA$ auxotroph's superior competitive ability for glucose using the inferred parameter set, which becomes limiting when sufficient tyrosine is externally supplied. Notably, this pattern of sensitivity can switch depending on moderate variations in the glucose utilization efficiency parameter values of each strain (Supplementary Fig. 7). This implies that the pattern of tyrosine supply sensitivity is not robust to variations in these parameters.

Dissecting the mechanisms that drive cycles

The mathematical analysis of our full model is hindered by the complexity arising from its five variables. To more deeply understand the mechanism driving the cyclic population dynamics, we reduce it to a minimal model for the two amino acids (R_1 and R_2) and the relative abundance of the two auxotrophs, $f = N_1/(N_1 + N_2)$ (a full derivation is provided in Supplementary Note 4). This minimal model captures the essential features of our system, shows similar dynamics to equation (1) (Supplementary Fig. 8), and is more amenable to analytical methods. This analysis of the minimal model identifies the cycles as relaxation oscillations, which show fast-slow dynamics^{37,38}, as have been identified in some predator-prey models³⁹. Based on the inferred parameter values, resource dynamics occur on a fast timescale. Therefore, the resource dynamics track a quasi-steady state determined by the relative abundance, f , punctuated by brief periods of rapid change. If the positive feedback due to resource cross-inhibition is stronger than negative feedback due to self-damping (growth-imposed resource limitation), the fast resource dynamics can show two alternative stable metabolic states. In each alternative state, one consumer auxotroph is glucose-limited, so it does not release amino acids. The other producer auxotroph is consequently limited by its required amino acid and therefore releases the amino acid it produces, which fuels growth of the consumer. This matches the experimentally observed monoculture resource dynamics (Fig. 2). The asymmetric cross-feeding relationship between the auxotrophs drives the strain relative abundance dynamics on a slower timescale. As the relative abundance of the producer auxotroph decreases, the amino acid concentrations track the stable resource equilibrium until it vanishes at a saddle-node bifurcation (Supplementary Fig. 9). This triggers an abrupt jump to the alternative resource equilibrium where the roles of producer and consumer auxotroph are reversed. Simulation of the full model (Eq. (1)) shows similar dynamics (Fig. 4) except for a brief period where both amino acids are being produced that coincides with the switch between alternative metabolic states (Fig. 4b iii and vi).

The minimal model provides insights into the parameter conditions that produce cycles. Linear stability analysis shows that $q_{11}q_{22} > q_{12}q_{21}$ is a necessary but not sufficient condition for existence of the alternative stable states in the fast resource-subsystem that are required for relaxation oscillations (Supplementary Note 4). The parameters q_{11} and q_{22} represent the strength of the positive feedback loop generated by resource cross-inhibition, while q_{12} and q_{21} represent the strength of the negative feedback due to self-damping. To evaluate whether this condition can predict the emergence of oscillations in the full model (eq. (1)), we randomly sampled values for q_{ij} and determined the qualitative behavior of the system for each parameter set (Fig. 3c). Our results from the full model were consistent with the condition derived from the minimal model. In addition, increasing the chemostat dilution rate D contributes to self-damping of the resources (i.e., negative feedback), which reduces the likelihood of alternative stable steady states and therefore cycles. In sum, our findings highlight the critical role that resource feedbacks operating on different

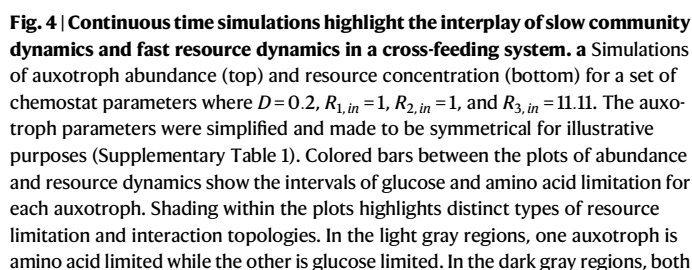
timescales play in shaping the complex dynamical behaviors of microbial communities.

Cycling between alternative stable states enables resistance to invasion

The capacity of a microbial community to resist invasion by cheater strains (i.e., strains that can benefit from public goods but do not produce them) plays a critical role in the stability and functionality of natural and engineered microbial communities^{40,41}. Using mathematical models, previous studies have shown that communities of cross-feeding auxotrophs can be vulnerable to invasion by a cheater that consumes both exchanged resources without participating in their production (e.g., dual auxotroph)²⁵. In certain parameter regimes, when the community reaches a stable equilibrium, the cheater can successfully invade by depleting the shared resources (public goods). As the resource is depleted, the producer strains become extinct, and thus the community collapses. Crucially, a successful cheater invasion can occur because both resources are available simultaneously, allowing the cheater to grow unimpeded. Notably, spatial separation of these resources through local interactions (microbe and resource dispersal) within the community can prevent the cheater from destabilizing the community by limiting access to at least one resource across different spatial locations⁴². We hypothesized that the temporal separation of required resources (Fig. 4a) could similarly block invasion of a dual auxotroph cheater by preventing simultaneous access to both amino acids.

To test this idea, we simulated an invasion of a dual auxotroph cheater in our chemostat model where cross-feeding is obligatory (no external amino acid supply) (Fig. 5a). Consistent with previous experimental research⁴³, we assume that the loss of both biosynthetic pathways in the cheater confers a moderate fitness advantage, enabling it to outcompete either of the single auxotrophs for limiting glucose in the presence of unlimited amino acids. Our simulations demonstrate that when the parameters were set to achieve a stable equilibrium, i.e., $q_{11}q_{22} < q_{12}q_{21}$, the cheater could invade the resident community and cause collapse through depletion of the exchanged resources (Fig. 5b, d and Supplementary Table 1). This also occurred when the parameters permitted oscillations ($q_{11}q_{22} > q_{12}q_{21}$) and the system resides at an unstable steady state (Supplementary Fig. 10a). In these stable equilibrium cases, both amino acids are produced simultaneously and thus can be exploited by the cheater strain. With all community members limited by amino acids, the moderate fitness advantage of the cheater strain enables it to outcompete the resident strains, eventually causing community collapse as the producer strains become extinct (Fig. 5f).

By contrast, for parameter values that lead to oscillations ($q_{11}q_{22} > q_{12}q_{21}$) the cheater is unable to successfully invade following its introduction (Fig. 5c and Supplementary Fig. 10b). The exclusion of the cheater occurs when the production of the exchanged resources (i.e., amino acids) are temporally separated, such that only one is available at any given time (Fig. 5e). Since the cheater requires both amino acids, its growth is always amino acid limited. During one phase of the oscillation, both the cheater and the $\Delta tyrA$ auxotroph are limited by tyrosine, although phenylalanine is abundant. During the subsequent phase of the oscillation, the cheater strain and $\Delta pheA$ are limited by phenylalanine, while tyrosine is abundant. Therefore, amino acid limitation at each phase of the oscillation results in a persistent negative net growth rate of the cheater. The specific growth rate of the cheater strain will only ever be slightly higher than the slowest growing member from the resident community (Fig. 5g). Over time, the abundance of the cheater is gradually reduced through dilution in the chemostat as the resident community continues to cycle between two metabolic states. Consistent with our simulation results, this invasion outcome was confirmed experimentally in our oscillating community (Supplementary Note 5 and Supplementary Fig. 11).



during periods of limitation by the required amino acid. This strategy could be explained by an endogenous stress response mechanism in *E. coli* in which specific amino acids, including the aromatics, accumulate during starvation because of protein degradation^{29,44,45}. As an alternative explanation, the observed resource dynamics could be an indirect consequence of the auxotrophic gene knockouts. Metabolic flux intended to remedy starvation of the required amino acid could

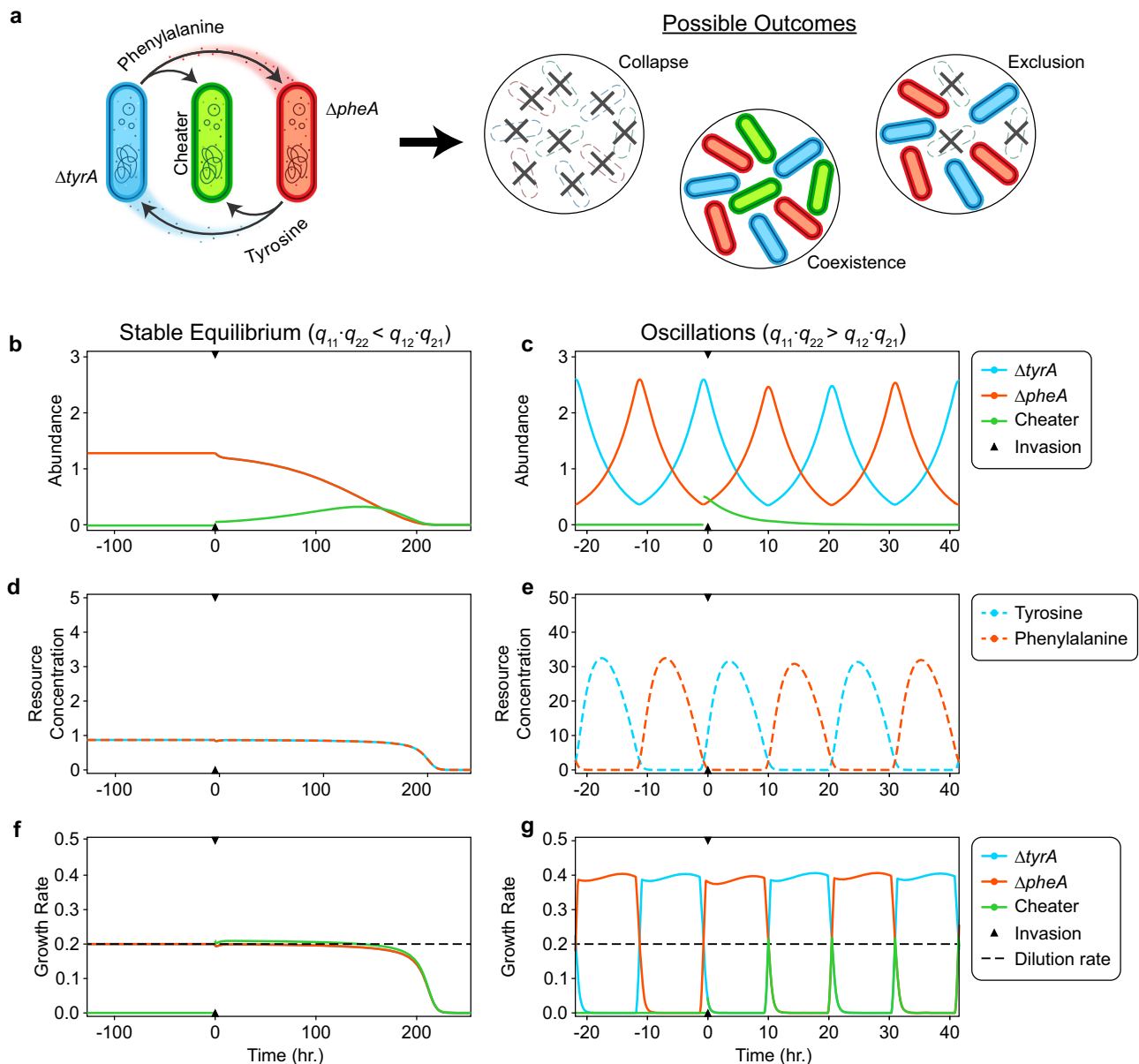


Fig. 5 | Temporal resource separation can prevent invasion and community collapse by a dual auxotroph cheater. **a** Two *E. coli* single amino acid auxotrophs exhibit mutually beneficial cross-feeding. A third community member having both amino acid auxotrophies consumes both exchanged resources but does not participate in their production. Introduction of the cheater to the cross-feeding resident community has three possible outcomes: (1) collapse of the entire community, (2) coexistence of the cheater and resident community, and (3) exclusion of the cheater by the resident community. **b, c** Simulations of the resident community at

steady state are perturbed at $t=0$ by introduction of the cheater. The initial abundance of the cheater was set at 0.05 in the stable equilibrium case and 0.5 in the oscillatory case. **d, e** Amino acid concentrations in the stable equilibrium and oscillating communities. **f, g** Specific growth rates of the community members in the stable equilibrium and oscillating communities. The dilution rate through the chemostat is shown as a black dashed line to highlight the periods during which each community member shows a net positive growth rate.

potentially leak into an overlapping pathway (Supplementary Note 2). Indeed, the anabolic pathways for tyrosine and phenylalanine are nearly identical, with only the final two reactions being distinct, suggesting that dysregulation of one pathway could impact the metabolic fluxes of the other pathway. Beyond the specific mechanism, the resulting cross-inhibition (Fig. 2h, i) captured in our models is essential to the oscillations in our system. Further, similar features of our system may occur more broadly in ecological systems shaped by resource exchange beyond microbial communities. For instance, a plant growth model with separate root and shoot compartments that share excess resources

(nitrogen and carbon) shows similar dynamics, alternating between two metabolically distinct states^{46,47}.

Although the interaction between strains is mutualistic (+/+) when averaged over an entire cycle, at most instants one auxotroph benefits without concurrently returning the favor, representing a transient commensalism. Due to the oscillations, species take turns as they alternate out of phase between disjoint periods of growth and amino acid resource production (Fig. 4a). Such dynamics mirror reciprocal altruism, where each strain temporarily sacrifices its growth to benefit the other, ensuring long-term mutual benefit⁴⁸.

The daily dilution in our experiments imposes a large perturbation on the system. Our chemostat model shows that the cycles observed experimentally do not require periodic external forcing, but the interaction between internal cyclic dynamics and external forcing has been shown to lead to complex dynamics in other systems^{13,35,38}. We explore this interaction by varying the dilution frequency while targeting a constant biomass through control of the dilution factor (Supplementary Note 3). For frequent and small dilutions, the dynamics resemble slight variation around the unforced limit cycle in our chemostat model. By contrast, larger, less-frequent dilutions generate integer-periodic dynamics mirroring our experiment (Supplementary Figs. 12 and 13). This connects our idealized continuous model with our experiments and suggests avenues for future exploration. For instance, future work could explore how specific patterns of environmental forcing, e.g., fluctuating resource supply, transient perturbations, or shifts in dilution frequency, could be used to control community dynamics.

Our focus on a single two-member cross-feeding community allowed us to dissect the feedback mechanisms driving population cycles. This detailed characterization may be more challenging in complex communities due to more complex pairwise and higher-order interaction mechanisms. As such, future work could examine whether similar dynamical behaviors emerge in other cross-feeding pairs, or in communities with three or more interacting members. In addition, future work could adopt a more systematic approach to screening strains by estimating resource production and consumption parameters in monoculture and identifying pairs of strains likely to exhibit oscillations based on the criterion $q_{ij}q_{ji} > q_{ji}q_{ij}$. Our model could then be used to guide the selection of amino acid supplementation concentrations tested experimentally in search of population cycles. Similar models could also be constructed to represent various interacting topologies in three-member communities, which could be computationally explored for oscillatory dynamics.

Our findings offer insights into how microbial communities could be engineered to achieve stable yet dynamic coexistence through reciprocal feedback-mediated resource exchange. The feedback loops in this system establish cooperation via nutrient limitation. This mechanism could inspire novel strategies for engineering the dynamics of synthetic microbial communities. For example, the efficiency and robustness of applications such as biomanufacturing and waste remediation could benefit from division-of-labor strategies that emerge naturally from self-organized oscillations⁴⁹. Further, the temporal patterning of public goods associated with population cycling could block cheater mutants from establishing, whether arising internally through evolution or introduced externally via dispersal. Consistent with this notion, $\Delta pheA$ displayed an abrupt increase in growth in certain replicates, potentially due to mutations (Fig. 1d, left). These dynamics were only observed in stable equilibrium conditions and destabilized the community. By contrast, all oscillating communities followed the same predictable trajectory (Fig. 1d, middle), suggesting oscillations might confer enhanced robustness and stability. Looking ahead, the ability to tune population cycles by adjusting environmental parameters such as external resource concentrations suggests that this mechanism could be exploited for sense-and-respond functionalities in living cellular therapeutics⁵⁰. More broadly, our work highlights how intrinsic feedback-mediated resource exchange can lead to rich and complex dynamical behaviors with potential applications in microbial engineering, synthetic ecology, and even programmable therapeutic consortia.

Methods

Strains

Strains used for all experiments were *E. coli* K-12 BW25113 single amino acid auxotrophs derived from the Keio Knockout Collection⁵¹. Deletion of the *tyrA* and *pheA* genes established the tyrosine and phenylalanine auxotrophies, respectively. Each auxotroph was transformed with a pBbA6c plasmid⁵² harboring a chloramphenicol resistance gene for

plasmid maintenance, and an isopropyl β -D-1-thiogalactopyranoside (IPTG) inducible fluorescence marker. The auxotrophs were transformed such that $\Delta tyrA$ expressed CFP and $\Delta pheA$ expressed RFP.

Construction of cheater strain

To construct a cheater strain, $\Delta tyrA$ and $\Delta pheA$ double knockout mutant, we employed the same recombineering strategy used in the construction of the Keio collection⁵¹. First, to enable selection via kanamycin resistance, the existing antibiotic resistance cassette in the $\Delta pheA$ background was removed using the FLP recombinase-mediated excision system⁵³. Briefly, cells were transformed with the FLP recombinase-expressing plasmid pFLP2 (NovoPro V006225), and the expression of FLP was induced to excise the cassette flanked by FRT sites. The pFLP2 plasmid was subsequently cured by growth at 37 °C. A PCR product containing a kanamycin resistance cassette flanked by FRT sites and 50-bp homology arms targeting *tyrA* was generated from the pKD4 (Addgene plasmid #45605) plasmid using primers: Forward, 5'-GATGATGTGAATCATCCGGCACTGGATTATTACTGGCGATTGTCATTCGCTGTAGGCTGGAGCTGCTTCG-3'; Reverse, 5'-GGATCTGAACGGGCAGCTGACGGCTCGCGTGGCTTAAGAGGTTTATTATG-3'. This PCR fragment was introduced into $\Delta pheA$ lacking a kanamycin cassette and harboring the λ -Red recombinase expression plasmid pMP11 (Addgene plasmid #215559). Cells were grown in LB media containing 1 mM L-arabinose at 30 °C to induce λ -Red expression and prepared as electroporation-competent cells. Electroporation was performed with 400 ng of PCR product in a 0.2 cm cuvette using a Bio-Rad electroporator (2.5 kV, 25 μ F, 200 Ω). After electroporation, cells were immediately recovered in 1 ml of SOC media (2% Bacto Tryptone, 0.5% yeast extract, 10 mM NaCl, 2.5 mM KCl, 10 mM MgCl₂, 10 mM MgSO₄, 20 mM glucose) and incubated for 1 h at 30 °C. Transformants were selected by plating one-tenth of the culture on kanamycin and ampicillin containing LB agar and incubating overnight at 30 °C. The pMP11 plasmid was cured by subsequent overnight growth at 37 °C. Finally, the cheater strain was transformed with a pBbA6c plasmid harboring IPTG inducible GFP fluorescence marker.

Preculture conditions

For each experiment involving the $\Delta tyrA$ or $\Delta pheA$ auxotrophs, pre-cultures were prepared by inoculating EZ Rich Defined Media (Teknova, #M2105) (Supplementary Table 3) containing 25 μ g/mL chloramphenicol with approximately 2 μ L of the appropriate glycerol stock. Cultures were then incubated for 16 h at 37 °C with 250 RPM orbital shaking. Cultures were then centrifuged for 5 min at 3000 $\times g$, and the cell pellet was washed once with MOPS Minimal Media (Teknova, #M2106) prior to resuspension.

Microscopy and cell counting

Absolute abundance measurements of the auxotrophs in co-culture were determined by combining OD₆₀₀ reading of the co-culture with relative abundance measurements. Relative abundance was measured using epifluorescence microscopy and a cell counting script that categorizes and counts cells based on their fluorescent label. For each culture, a 2 μ L sample was spotted onto a glass slide treated with poly-L-lysine (Sigma, #P8920) and covered with a glass coverslip. Microscopy was performed on a Nikon Eclipse Ti where two regions of interest were imaged for each sample using a 20X objective. Each image was composed of a phase contrast channel, an ECFP channel for $\Delta tyrA$ identification (Nikon, #96361, 436 \times 20 nm excitation/480 \times 40 nm emission), and an mCherry channel for $\Delta pheA$ identification (Nikon, #96365, 560 \times 40 nm excitation/630 \times 70 nm emission), and a FITC channel for cheater identification (Nikon, #96242, 470 \times 40 nm excitation/534 \times 55 nm emission).

The total number of cells in each fluorescence channel was counted using ImageJ and Nikon imaging software (NIS-Elements AR, version 4.51). In ImageJ, an automated script applied a Gaussian

blur filter ($\sigma=1$) before using the Find Maxima function for individual cell identification. A peak prominence value of 300 was set for the Find Maxima function, and cells located at the image edges were excluded from the final count. For the cheater invasion experiment (Supplementary Note 5 and Supplementary Fig. 11), cell numbers were measured automatically in the Nikon imaging software using the “Binary” tool with a size threshold ($<4\ \mu\text{m}$) to exclude debris and non-cellular artifacts. CFP-, RFP-, and GFP-expressing cells were quantitatively counted using the “Automated Measurement” tool, applying fluorescence intensity thresholds of 250, 2000, and 2000 (arbitrary units), respectively. Quantitative data were further analyzed and visualized using Python’s Matplotlib and Seaborn packages. All measurements were performed in triplicate. Our microscopy based relative abundance measurements were validated with the same measurements made via colony forming unit (CFU) measurements ($\rho=0.9928$, $p=1.4619\text{e}-10$) (Supplementary Fig. 14).

Obligate exchange experiment

Precultures of ΔtyrA and ΔpheA were diluted into 1 mL of fresh MOPS Minimal Media (Teknova #M2106) (Supplementary Table 3) containing $25\ \mu\text{g}/\text{mL}$ chloramphenicol and 1 mM IPTG as monocultures and a pairwise coculture. Each culture was inoculated to achieve a total optical density at 600 nm (OD_{600}) of 0.1. For the coculture, the inoculum ratio of the two auxotrophs was 1:1. All cultures were then incubated for 24 h at 37°C with 250 RPM orbital shaking. Following incubation, the OD_{600} of each culture was measured. Relative abundance was also measured in the community culture using epifluorescence microscopy (Nikon Eclipse Ti) and an automated cell counting script (ImageJ). Absolute abundance of each strain was calculated by multiplying the relative abundance measurements with the OD_{600} of the community.

Batch passaging experiments

Stock solutions of L-tyrosine (Sigma-Aldrich, #T3754) and L-phenylalanine (Dot Scientific, #DSP20260) were prepared in Milli-Q water, and subsequently used to prepare supplemented MOPS Minimal Media. The tyrosine stock solution was prepared at a 1 mM concentration in warm water with 1 h of sonication to facilitate dissolution. The phenylalanine stock solution was prepared at a 40 mM concentration with stirring. For the initial batch passaging experiment (Fig. 1d), the amino acid supply concentrations were either 0 μM , 10 μM , or 20 μM for tyrosine, and 0 μM , 10 μM , or 20 μM for phenylalanine. For the expanded batch passaging experiment (Extended Data Fig. 1), the supply concentrations of tyrosine were 0 μM , 5 μM , 10 μM , 20 μM , 40 μM , or 80 μM , while the concentrations of phenylalanine were 0 μM , 10 μM , 20 μM , 40 μM , 80 μM , or 160 μM .

For all batch passaging experiments, precultures of ΔtyrA and ΔpheA were diluted into 1 mL of fresh media ($n=3$) containing $25\ \mu\text{g}/\text{mL}$ chloramphenicol and 1 mM IPTG as pairwise communities. The total OD_{600} of the inoculum was equal to 0.1 for all conditions. Communities were established at a ratio of 9:1 (ΔtyrA to ΔpheA). This inoculum bias was introduced to synchronize the oscillation phase across replicates and was not necessary for the development of oscillations (Supplementary Fig. 15). Cultures were then incubated at 37°C with 250 RPM orbital shaking and passaged every 24 h to an OD_{600} of 0.1 in fresh media. At each passage, the relative abundance of each auxotroph was measured using epifluorescence microscopy (Nikon Eclipse Ti) and an automated cell counting script (ImageJ).

Cheater strain invasion analysis during batch passaging

The cheater strain was introduced during the batch passaging experiments between Day 3 and Day 4. Specifically, the fourth passage was inoculated in fresh media with OD_{600} of 0.15, composed of 0.1 OD_{600} of the previous passage and 0.05 OD_{600} of the cheater strain. Subsequent passages were performed by transferring a total OD_{600} of 0.1, consistent with the batch passaging experiment. At each passage,

the relative abundances of the ΔtyrA , ΔpheA , and cheater strains were quantified using Nikon imaging software.

Amino acid and glucose profiling experiment

Precultures of ΔtyrA and ΔpheA were diluted as monocultures ($n=3$) into 4 mL of fresh MOPS Minimal Media (Teknova, #M2106) containing $25\ \mu\text{g}/\text{mL}$ of chloramphenicol. Monocultures of ΔtyrA were supplemented with either 10 μM , 20 μM , or 200 μM of tyrosine, and ΔpheA was supplemented with either 20 μM , 40 μM , or 400 μM of phenylalanine. Following inoculation, the cultures were incubated with shaking for 24 h ($37^\circ\text{C}/250\ \text{RPM}$). Every 2 h during the first 12 h of incubation, the OD_{600} of each culture was measured using a NanoDrop spectrophotometer (Thermo, #ND-ONEC-W), and 300 μL samples were extracted for further processing.

Purified conditioned media were obtained from each sample through centrifugation and aspiration of the supernatant, followed by filtration using a 0.2 μm hydrophilic polyethersulfone membrane (Pall, #8019). A final set of samples was obtained at 24 h of incubation.

Quantitation of tyrosine, phenylalanine, and glucose in the purified conditioned media samples was achieved with separate enzymatic assay kits and a multimode microplate reader (Tecan Spark). Tyrosine was quantified with a colorimetric kit (Cell Biolabs, #MET5073), phenylalanine was quantified with a fluorometric kit (bioAssay Systems, #EPHE100), and glucose was quantified with a fluorometric kit (Invitrogen, #A22189).

Intrabatch dynamics experiment

Precultures of ΔtyrA and ΔpheA were used to inoculate 1 mL of fresh MOPS Minimal Media (Teknova, #M2106) supplemented with 10 μM tyrosine, 20 μM phenylalanine, 1 mM IPTG, and $25\ \mu\text{g}/\text{mL}$ chloramphenicol with three replicates for each condition. The inoculum ratio of ΔtyrA to ΔpheA was 1:9, and the total community OD_{600} was equal to 0.1. Cultures were then incubated at 37°C with 250 RPM orbital shaking and passaged every 24 h by diluting the culture to an OD_{600} of 0.1 at the beginning of each passage. At each passage, the community composition was analyzed using epifluorescence microscopy (Nikon Eclipse Ti) and an automated cell counting script (ImageJ). Daily passages into fresh media and measurements of auxotroph abundance proceeded for a total of 6 days.

During the fifth and sixth batches, samples of each culture were taken every 2 h for the initial 8 h, then once more at 24 h. Sampling within the batch was performed without passaging, and steps were taken to minimize the duration that cultures were outside of the incubator. Each sample consisted of 10 μL , of which 2 μL was used for relative abundance quantification with epifluorescence microscopy, and another 2 μL was diluted to 20 μL for quantification of OD_{600} with a NanoDrop spectrophotometer (Thermo, #ND-ONEC-W).

Parameter inference

The differential equation model (Eq. (1)) was fit to the experimental data shown in Fig. 1d using the *fmincon* function in MATLAB (R2022a), which minimizes a constrained nonlinear multivariable objective function. We constructed an objective function that simulates the passaging experiment using *ode89* and predicts auxotroph abundance values corresponding with the data presented in Fig. 1d. The L2-norm of the residuals, defined as the difference between the predicted and measured abundance values, was added to a regularization error as the net output from the objective function. The regularization error was computed from the L1-norm of the parameter set. A best estimate weighting scheme was applied to the parameter values during regularization to account for the differences in parameter value magnitudes. This scheme normalizes each parameter according to its weight prior to computing the L1-norm. Parameter weights were derived from the average parameter value taken over a series of manually selected parameter sets that produced qualitatively accurate results. Finally, the

L1-norm was multiplied by a regularization parameter (λ) to scale the regularization error.

Due to the sensitivity of the optimization to the initial conditions, we independently varied the regularization parameter and the initial parameter guess. The initial parameter sets were constructed from a Latin hypercube sampling design where the bounds were determined from a manually selected set of parameter sets. All parameters were assigned a non-negative constraint, while $\mu_{1, \max}$ and $\mu_{2, \max}$ were also assigned an upper bound constraint.

Once the parameter optimizations were complete for all regularization parameters and all initial parameter sets, the optimized parameter sets were evaluated against a validation dataset (Supplementary Fig. 2), and the final parameter set was selected based on the lowest overall mean squared error across the training and validation datasets.

Bifurcation analysis

Bifurcation analysis was performed using the inferred parameter sets (Supplementary Tables 1 and 2). Direct model simulations were performed to obtain the steady-state community compositions for each set of amino acid supplementation concentrations. Hopf, fold, and transcritical bifurcations were identified and followed using numerical continuation in MatCont⁵³ using the default integration parameters.

Statistical analysis

Statistical analyses were performed where appropriate to highlight significant differences between experimental conditions. Statistical comparisons are indicated in all relevant figures, using standard significance markers (* $p < 0.05$; ** $p < 0.01$; *** $p < 0.001$; n.s., not significant). Exact p values are reported in the corresponding figure legends. Where applicable, a corrected Hedges' effect size (g^*) is provided for each p -value.

Unpaired two-tailed t -tests were performed to compare measurements across different amino acid supplementation regimes and other experimental treatments (Fig. 1b). For Fig. 1d, a t -test was used to assess the presence of period-two oscillations in the absolute abundance dynamics of the two-member co-culture. To do this, we compared the average community composition ratio ($\Delta\text{tyrA}/\Delta\text{pheA}$) between even and odd days, beginning on day 3 to allow transient dynamics to settle. A significant difference between these groups supports the presence of alternating populations observed in period-two oscillations.

For binary classification of amino acid presence/absence based on the analytical limit of detection (LOD), generalized estimating equations (GEE) with a binomial distribution and exchangeable correlation structure were used to model the probability of released amino acid presence as a function of required amino acid availability (Fig. 2h, i). This approach accounts for potential correlations between measurements made on a single culture over time. The model includes an intercept and a binary predictor indicating the presence/absence of required amino acid. Coefficients were estimated using quasi-likelihood methods, and significance was determined using Wald tests. Confidence intervals (95%) were computed by transforming the linear predictor and its standard error into the probability scale using the logistic function.

Reporting summary

Further information on research design is available in the Nature Portfolio Reporting Summary linked to this article.

Data availability

Source data for Figs. 1b, d, and 2b–g, and Supplementary Figs. 1, 2, 3, 5, 6, 11, 14, 15, and 16, can be found in the Source Data file. Source data for Fig. 1d can also be found in the publicly available GitHub repository https://github.com/VenturelliLab/Ross_et_al_2025⁵⁴ along with the associated scripts for model fitting and data plotting. The GitHub repository also contains the key parameter sets used for model simulations in producing Figs. 1d, 3b, c, 5b–g, and Supplementary Figs. 2, 3, 5, 10, 11, 12, and 13. All data used in this work are original and

were generated internally; no previously published datasets were reused. Source data are provided with this paper.

Code availability

Code for fitting the dynamical models, producing model predictions, and simulating cheater invasion experiments is publicly available at the following GitHub repository https://github.com/VenturelliLab/Ross_et_al_2025⁵⁴. The repository includes all scripts and associated documentation necessary to reproduce key results.

References

- Kendall, B. E. et al. Why do populations cycle? A synthesis of statistical and mechanistic modeling approaches. *Ecology* **80**, 1789–1805 (1999).
- Lotka, A. *Elements of Physical Biology* (Williams and Wilkins Company, 1925).
- Volterra, V. *Variazioni e Fluttuazioni Del Numero d'individui in Specie Animali Conviventi* (Società Anonima Tipografica Leonardo da Vinci, 1926).
- Turchin, P. *Complex Population Dynamics: A Theoretical/Empirical Synthesis* (Princeton University Press, 2003).
- McCauley, E., Nelson, W. A. & Nisbet, R. M. Small-amplitude cycles emerge from stage-structured interactions in Daphnia–algal systems. *Nature* **455**, 1240–1243 (2008).
- Kerr, B., Riley, M. A., Feldman, M. W. & Bohannan, B. J. M. Local dispersal promotes biodiversity in a real-life game of rock–paper–scissors. *Nature* **418**, 171–174 (2002).
- Yoshida, T., Jones, L. E., Ellner, S. P., Fussmann, G. F. & Hairston, N. G. Rapid evolution drives ecological dynamics in a predator–prey system. *Nature* **424**, 303–306 (2003).
- Qian, J. J. & Akçay, E. The balance of interaction types determines the assembly and stability of ecological communities. *Nat. Ecol. Evol.* **4**, 356–365 (2020).
- Kouzuma, A., Kato, S. & Watanabe, K. Microbial interspecies interactions: recent findings in syntrophic consortia. *Front. Microbiol.* **6**, 135778 (2015).
- Kost, C., Patil, K. R., Friedman, J., Garcia, S. L. & Ralser, M. Metabolic exchanges are ubiquitous in natural microbial communities. *Nat. Microbiol.* **8**, 2244–2252 (2023).
- Vandermeer, J. H. & Boucher, D. H. Varieties of mutualistic interaction in population models. *J. Theor. Biol.* **74**, 549–558 (1978).
- Gokhale, S., Conwill, A., Ranjan, T. & Gore, J. Migration alters oscillatory dynamics and promotes survival in connected bacterial populations. *Nat. Commun.* **9**, 5273 (2018).
- Yurtsev, E. A., Conwill, A. & Gore, J. Oscillatory dynamics in a bacterial cross-protection mutualism. *Proc. Natl. Acad. Sci.* **113**, 6236–6241 (2016).
- Boucher, D. H. Lotka-volterra models of mutualism and positive density-dependence. *Ecol. Model.* **27**, 251–270 (1985).
- May, R. M. *Theoretical Ecology: Principles and Applications* (Sinauer Associates, 1981).
- Hale, K. R. S. & Valdovinos, F. S. Ecological theory of mutualism: Robust patterns of stability and thresholds in two-species population models. *Ecol. Evol.* **11**, 17651–17671 (2021).
- Falkowski, P. G., Fenchel, T. & Delong, E. F. The microbial engines that drive earth's biogeochemical cycles. *Science* **320**, 1034–1039 (2008).
- Hou, K. et al. Microbiota in health and diseases. *Signal Transduct. Target Ther.* **7**, 135 (2022).
- D'Souza, G. et al. Less is more: selective advantages can explain the prevalent loss of biosynthetic genes in bacteria. *Evolution* **68**, 2559–2570 (2014).
- D'Souza, G. et al. Ecology and evolution of metabolic cross-feeding interactions in bacteria. *Nat. Prod. Rep.* **35**, 455–488 (2018).
- Harcombe, W. Novel cooperation experimentally evolved between species. *Evolution* **64**, 2166–2177 (2010).

22. Pande, S. et al. Fitness and stability of obligate cross-feeding interactions that emerge upon gene loss in bacteria. *ISME J.* **8**, 953–962 (2014).
23. Oña, L. et al. Obligate cross-feeding expands the metabolic niche of bacteria. *Nat. Ecol. Evol.* **5**, 1224–1232 (2021).
24. Mee, M. T., Collins, J. J., Church, G. M. & Wang, H. H. Syntrophic exchange in synthetic microbial communities. In *Proc. National Academy of Sciences* **111**, (PNAS, 2014).
25. Sun, Z., Koffel, T., Stump, S. M., Grimaud, G. M. & Klausmeier, C. A. Microbial cross-feeding promotes multiple stable states and species coexistence, but also susceptibility to cheaters. *J. Theor. Biol.* **465**, 63–77 (2019).
26. Hoek, T. A. et al. Resource availability modulates the cooperative and competitive nature of a microbial cross-feeding mutualism. *PLoS Biol.* **14**, e1002540 (2016).
27. Chesson, P. MacArthur's consumer-resource model. *Theor. Popul. Biol.* **37**, 26–38 (1990).
28. Hart, S. F. M. et al. Uncovering and resolving challenges of quantitative modeling in a simplified community of interacting cells. *PLoS Biol.* **17**, e3000135 (2019).
29. Jozefczuk, S. et al. Metabolomic and transcriptomic stress response of *Escherichia coli*. *Mol. Syst. Biol.* **6**, 364 (2010).
30. Takano, S., Pawlowska, B. J., Gudelj, I., Yomo, T. & Tsuru, S. Density-dependent recycling promotes the long-term survival of bacterial populations during periods of starvation. *mBio* **8**, e02336–16 (2017).
31. Christopherson, R. I. Chorismate mutase-prephenate dehydrogenase from *Escherichia coli*: Cooperative effects and inhibition by L-tyrosine. *Arch. Biochem. Biophys.* **240**, 646–654 (1985).
32. Dopheide, T. A., Crewther, P. & Davidson, B. E. Chorismate mutase-prephenate dehydratase from *Escherichia coli* K-12. II. Kinetic properties. *J. Biol. Chem.* **247**, 4447–4452 (1972).
33. Duggleby, R. G., Sneddon, M. K. & Morrison, J. F. Chorismate mutase-prephenate dehydratase from *Escherichia coli*: active sites of a bifunctional enzyme. *Biochemistry* **17**, 1548–1554 (1978).
34. Pittard, J. & Yang, J. Biosynthesis of the aromatic amino acids. *EcoSal Plus* **3**, 7242 (2008).
35. Summers, D., Cranford, J. G. & Healey, B. P. Chaos in periodically forced discrete-time ecosystem models. *Chaos Solitons Fractals* **11**, 2331–2342 (2000).
36. Tilman, D. Resources: a graphical-mechanistic approach to competition and predation. *Am. Nat.* **116**, 362–393 (1980).
37. Ginoux, J.-M. & Letellier, C. Van der Pol and the history of relaxation oscillations: toward the emergence of a concept. *Chaos* **22**, 023120 (2012).
38. Strogatz, S. H. *Nonlinear Dynamics and Chaos* (CRC Press, 2018).
39. Ludwig, D., Jones, D. D. & Holling, C. S. Qualitative analysis of insect outbreak systems: the spruce budworm and forest. *J. Anim. Ecol.* **47**, 315 (1978).
40. Smith, P. & Schuster, M. Public goods and cheating in microbes. *Curr. Biol.* **29**, R442–R447 (2019).
41. Cavaliere, M., Feng, S., Soyer, O. S. & Jiménez, J. I. Cooperation in microbial communities and their biotechnological applications. *Environ. Microbiol.* **19**, 2949–2963 (2017).
42. Stump, S. M., Johnson, E. C. & Klausmeier, C. A. Local interactions and self-organized spatial patterns stabilize microbial cross-feeding against cheaters. *J. R. Soc. Interface* **15**, 20170822 (2018).
43. D'Souza, G. & Kost, C. Experimental evolution of metabolic dependency in bacteria. *PLoS Genet.* **12**, e1006364 (2016).
44. Reeve, C. A., Bockman, A. T. & Matin, A. Role of protein degradation in the survival of carbon-starved *Escherichia coli* and *Salmonella typhimurium*. *J. Bacteriol.* **157**, 758–763 (1984).
45. Link, H., Fuhrer, T., Gerosa, L., Zamboni, N. & Sauer, U. Real-time metabolome profiling of the metabolic switch between starvation and growth. *Nat. Methods* **12**, 1091–1097 (2015).
46. Ledder, G., Russo, S. E., Muller, E. B., Peace, A. & Nisbet, R. M. Local control of resource allocation is sufficient to model optimal dynamics in syntrophic systems. *Theor. Ecol.* **13**, 481–501 (2020).
47. Pfaf, F. et al. Timescale separation and models of symbiosis: state space reduction, multiple attractors and initialization. *Conserv. Physiol.* **10**, coac026 (2022).
48. Trivers, R. L. The evolution of reciprocal altruism. *Q. Rev. Biol.* **46**, 35–57 (1971).
49. McCarty, N. S. & Ledesma-Amaro, R. Synthetic biology tools to engineer microbial communities for biotechnology. *Trends Biotechnol.* **37**, 181–197 (2019).
50. Din, M. O. et al. Synchronized cycles of bacterial lysis for in vivo delivery. *Nature* **536**, 81–85 (2016).
51. Baba, T. et al. Construction of *Escherichia coli* K-12 in-frame, single-gene knockout mutants: the Keio collection. *Mol. Syst. Biol.* **2**, 2006.0008 (2006).
52. Lee, T. S. et al. BglBrick vectors and datasheets: a synthetic biology platform for gene expression. *J. Biol. Eng.* **5**, 12 (2011).
53. Dhooge, A., Govaerts, W., Kuznetsov, Y. A., Meijer, H. G. E. & Sautois, B. New features of the software MatCont for bifurcation analysis of dynamical systems. *Math. Comput. Model. Dyn. Syst.* **14**, 147–175 (2008).
54. Ross, T. & Klausmeier, C. Ross_et_al_2025. https://github.com/VenturelliLab/Ross_et_al_2025 <https://doi.org/10.5281/zenodo.16762299> (2025).

Acknowledgements

We thank Yili Qian for his early insight regarding modeling approaches and strategies for parameter inference. We thank Scott Coyle for assistance with microscopy experiments. This research was supported by the Department of Defense (W911NF-19-1-0269 to O.S.V.), the National Institutes of Health (R35GM124774 to O.S.V.), and the National Science Foundation (EF-2124800 to C.A.K.). The funding organizations were not involved in the design of the study, the collection and analysis of data, the decision to publish, or the preparation of the manuscript.

Author contributions

T.D.R. and O.S.V. designed the study; T.D.R., H.I., and B.G.K. performed the experiments; T.D.R., H.I., B.K., and O.S.V. analyzed the data; T.D.R. and C.A.K. developed the models; T.D.R., C.A.K. and O.S.V. analyzed the models and wrote the manuscript; O.S.V. supervised the research and secured funding.

Competing interests

The authors declare no competing interests.

Additional information

Supplementary information The online version contains supplementary material available at <https://doi.org/10.1038/s41467-025-63986-y>.

Correspondence and requests for materials should be addressed to Christopher A. Klausmeier or Ophelia S. Venturelli.

Peer review information *Nature Communications* thanks Samir Giri, Wenying Shou who co-reviewed with Jamila Rowland-Chandler, and the other anonymous, reviewer(s) for their contribution to the peer review of this work. A peer review file is available.

Reprints and permissions information is available at <http://www.nature.com/reprints>

Publisher's note Springer Nature remains neutral with regard to jurisdictional claims in published maps and institutional affiliations.

Open Access This article is licensed under a Creative Commons Attribution-NonCommercial-NoDerivatives 4.0 International License, which permits any non-commercial use, sharing, distribution and reproduction in any medium or format, as long as you give appropriate credit to the original author(s) and the source, provide a link to the Creative Commons licence, and indicate if you modified the licensed material. You do not have permission under this licence to share adapted material derived from this article or parts of it. The images or other third party material in this article are included in the article's Creative Commons licence, unless indicated otherwise in a credit line to the material. If material is not included in the article's Creative Commons licence and your intended use is not permitted by statutory regulation or exceeds the permitted use, you will need to obtain permission directly from the copyright holder. To view a copy of this licence, visit <http://creativecommons.org/licenses/by-nc-nd/4.0/>.

© The Author(s) 2025